To appear in *Vehicle System Dynamics*
Vol. 00, No. 00, Month 20XX, 1–19

The effect of Ackermann steering on the performance of race cars

M. Veneri and M. Massaro*

Department of Industrial Engineering, University of Padova,
Via Venezia 1, 35131 Padova, Italy

(*Received 00 Month 20XX; accepted 00 Month 20XX*)

While several papers dealing with the kinematic of mechanisms that approximate the well known Ackermann steering are available, apparently there are no contributions related to the effect of Ackermann steering on vehicle performance. The current work focuses on the effect of Ackermann steering and parallel steering on the performance of a racing car, after a discussion on the different definitions of Ackermann steering ratio available in the literature. Three scenarios are considered: steady turning, slalom and a circuit lap. Nonlinear optimal control techniques are employed to assess the maximum performance. A Formula SAE car model is used and validated against experimental data in acceleration, steady turning and slalom. Then the same model is employed to investigate the effect of different steering layouts.

Keywords: Ackermann steering; parallel steering; minimum time; race car; optimisation; optimal control; car dynamics.

1. Introduction

In 1759 Erasmus Darwin proposed a novel carriage steering mechanism based on steering each wheel rather than the entire front axle – the common practice at the time. This novel system improves comfort and safety and, due to the larger steering angle of the inner tyre, promotes a lower tyre scuffing [1, 2]. A few years later, the same idea was proposed in G. Lankensperger and patented by R. Ackermann in 1818. In 1878 C. Jeantaud proposed a four-bar linkage mechanism that approximates the Darwin's (or Ackermann's) steering geometry [2–4]. Nowadays different linkages are usually employed, whose characteristics are often compared against the Ackermann in terms of angle differences, angle ratios, etc. The Ackermann steering system is discussed in most vehicle dynamics books, see e.g. [2, 5–8]. It is also well known that the exact Ackermann steering may not be the ideal steering in many scenarios – indeed it was developed under the assumption of zero tyre slippage, which is not the case realised unless very low speeds are considered.

There are several contributions in the literature related to mechanisms capable of approximating the Ackermann steering geometry. In [9] the first analytical design of a planar Ackermann linkage is devised. The synthesis equations of a four-bar linkage are combined with the desired steering characteristics of the vehicle through an approximated relationship. In [10] the effect of the error related to the Ackermann steering approximation is investigated in relation to the tire wear measured in trucks. More recently, in [11] the optimisation of an Ackermann linkage is carried out, together with the

*Corresponding author. Email: matteo.massaro@unipd.it

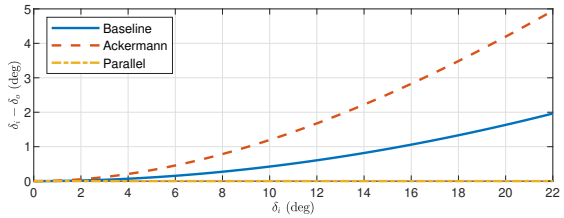

(a)

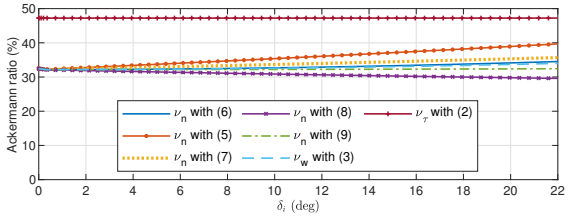

(b)

Figure 1.: a) Comparison between the different steering kinematic characteristics selected. FSAE current configuration (solid), Ackermann (dashed) and parallel (dash-dot). b) Comparison between different Ackermann-ratio definitions.

analysis of different target functions and the related parametric analysis. In [12] a novel Ackermann steering definition is proposed, with the aim of enhancing the Jeantaud approximation by including the effect of the steering tie-rod. The cornering performance of a four-wheel-steering vehicle model with independent front steering system is evaluated in [13]. At low lateral accelerations an Ackermann steering is deemed optimal, while at high lateral accelerations the outer wheel steering may need to be increased to enhance the cornering performance.

The aim of the current work is i) to summarise and compare the most widespread definitions of Ackermann steering ratio reported in the literature and ii) to assess the effect of such ratios on the performance of a race car. An FSAE car model is employed. Such model is validated against the road tests and then used to asses the performance of the Ackermann steering, parallel steering and baseline steering configurations. A nonlinear optimal control approach is employed to assess the maximum performance. Under this framework, the driver has perfect knowledge of the vehicle, tyre and road characteristics and is thus capable of reaching the physical limits. The nonlinear optimal control approach to the maximum performance of vehicles has been extensively discussed in the literature [2, 14–30].

The current work is organised as follows. In Section 2 the different definitions of Ackermann steering ratio reported in the literature are summarised and compared. In Section 3 the numerical vehicle and tyre models employed in this study are described and the related equations are reported. In Section 4 the nonlinear optimal control problem is built. In Section 5 the validation of the model against the road tests is shown. In Section 6 the effect of steering on the performance of the race car is investigated.

2. Steering geometry definitions

The terms ‘Ackermann steering’ or ‘Ackermann geometry’ refer to the

> steering system kinematics where the wheel-spin axes of the steerable wheels intersect the centre of rotation, for non-zero steering-wheel angles at negligible lateral accelerations [...] A steering system with Ackermann geometry is said to be 100 % Ackermann, and one with equal steer angles (parallel steer) on the steerable axle is said to be 0 % Ackermann. [31]

A standard and well-known derivation give the following relationship between the inner δ_i and outer δ_o wheel angles in the case of Ackermann steering

$$\frac{1}{\tan\delta_o} - \frac{1}{\tan\delta_i} = \frac{T}{w}, \tag{1}$$

where δ_o is the steering angle of the outer wheel, δ_i is the steering angle of the inner

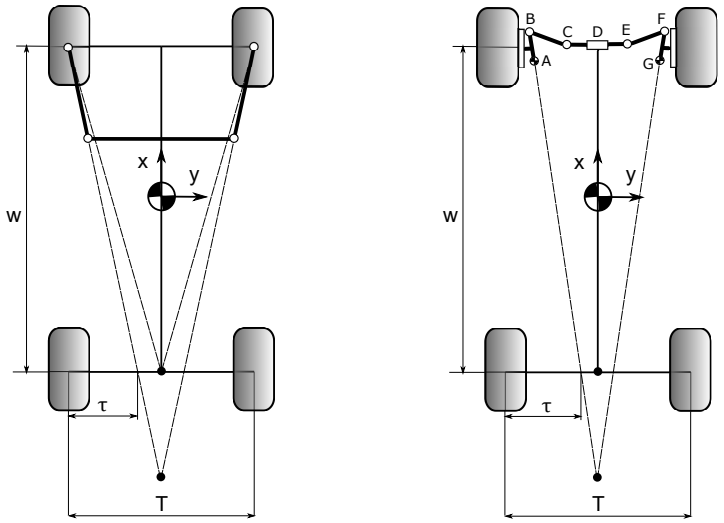

Figure 2.: a) Approximation of the Ackermann steering geometry using a four-bar linkages. b) Steering linkage of the FSAE vehicle under investigation.

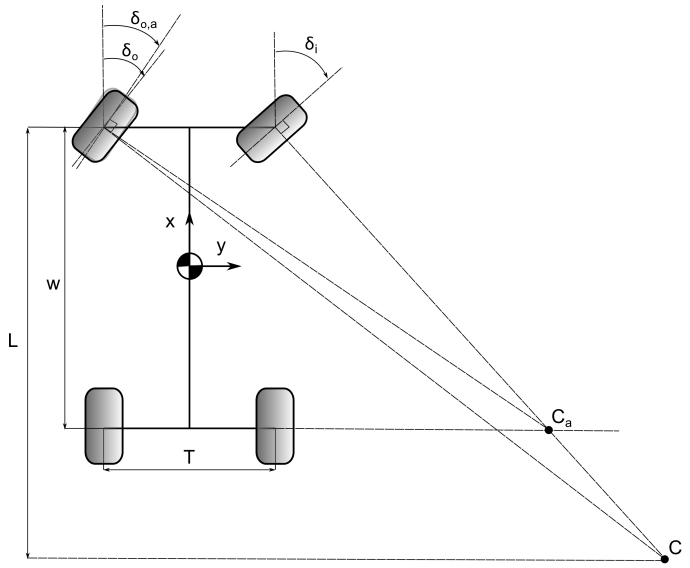

Figure 3.: Actual steering vs. Ackermann steering.

wheel, T is the track width and w is the wheelbase.

The comparison between the steering geometry used in the FSAE simulated car (baseline steering configuration), the Ackermann steering and the parallel steering is shown in Fig. 1a. The difference between the inner and outer wheel steering angles $\delta_i - \delta_o$ is shown at different internal wheel steering angles δ_i. When $\delta_i - \delta_o$ is negative (which never happens with the current setup), the geometry is said reverse-Ackermann [5, 7]. There are a number of different definitions in the literature when it comes to comparing the actual steering against the Ackermann steering. The most common definitions will now be concisely reviewed.

In 1878 C. Jeantaud proposed to approximate the Ackermann steering with a four-bar linkage mechanism that has two rockers pointing towards the middle of the rear axle; see Fig 2a. Such layout could thus be considered 100 % Ackermann. If the two rockers point below the middle of the rear axle, the steering is less then 100 % Ackermann, parallel steering is obtained when the two rockers are parallel, while if the two rockers point above the middle of the rear axle the steering is more than 100 % Ackermann. Finally, if the intersection of the two rockers moves in front of the front axle, reverse-Ackermann steering is obtained, i.e. the steer of the inner wheel is smaller that the steer of the outer wheel. The distance between the connecting rod and the line between the steering pivots does not affect the steering geometry for small steer rotations, as long as the inclination of the two rockers remains constant. Indeed, basic kinematic considerations dictate that the position of the velocity center of the connecting rod is at the intersection of the rockers' axes. The Ackermann steering ratio is sometimes computed as

$$\nu_\tau = \frac{\tau}{T/2}, \tag{2}$$

where τ is the distance between the intersection of the rocker axis and the rear axle, while T is the track width, see Fig. 2a.

In the current industrial practice, the Jeantaud layout is modified by replacing the connecting rod with two tie rods (CB and EF) that connect the wheel hub to the steering rack (CDE); see Fig. 2b. As in the case of the four-bar linkage, when the two rods AB and FG point towards the middle of the rear axle the layout could be considered 100 % Ackermann. The conditions of different Ackermann ratios follow the considerations reported for the Jeantaud linkage.

A different method for defining the steering geometry relates to the position of the projection of the velocity centre of the front wheels on the vehicle wheelbase [12]. In this case the Ackermann ratio is given by

$$\nu_w = \frac{w}{L}, \tag{3}$$

where L is shown in Fig. 3. If the projection is on the rear axle, the steering system is 100 % Ackermann. If the projection is below the rear axle ($L > w$) the layout is less than 100 % Ackermann, if the projection lies at infinity ($L = \infty$) the parallel steering is obtained (0 % Ackermann).

A net-steer ratio definition is often employed. This is the ratio of the difference between the inner and outer wheel-steering angles to the difference between the inner and outer wheel-steering angles of the corresponding Ackermann geometry

$$\nu_n = \frac{\delta_i - \delta_o}{\delta_{i,a} - \delta_{o,a}}, \tag{4}$$

where δ_i and δ_o are the inner and outer wheel-steering angles of the current layout, while $\delta_{i,a}$ and $\delta_{o,a}$ are the inner and outer wheel-steering angles in the corresponding Ackermann geometry. There are two main widespread options to identify the Ackermann geometry associated to the current steering geometry. In the first option, the inner wheel-steering angle is kept fixed and equal to the inner-wheel steering angle of the current layout, i.e. $\delta_{i,a} = \delta_i$, while the outer wheel-steering angle of the Ackermann geometry is readily computed from (1) as

$$\delta_{o,a} = \arctan\left(\frac{w\tan\delta_{i,a}}{w + T\tan\delta_{i,a}}\right). \tag{5}$$

In the second option, both the inner-wheel and outer-wheel steering angles are changed by the same quantity t in order to give the Ackermann steering geometry, i.e.

$$\delta_{i,a} = \delta_i + t, \qquad \delta_{o,a} = \delta_o - t. \tag{6}$$

In other words, in this case the Ackermann steering is obtained by applying a toe correction to the current steering layout. Such correction can be either positive (toe-out) or negative (toe-in) and is not constant. The latter option is employed e.g. in [32, 33].

Finally, a linearised version of the net-steer ratio (4) is sometime used [12]. In this case the denominator of (4) is approximated with the following expression which is obtained from (1)

$$\delta_{i,a} - \delta_{o,a} \approx \delta_o\delta_i\frac{T}{w} \approx \delta_o^2\frac{T}{w}. \tag{7}$$

Alternatively, the term δ_o^2 in (7) can be replaced by δ_i^2

$$\delta_{i,a} - \delta_{o,a} \approx \delta_i^2\frac{T}{w}. \tag{8}$$

or by δ_m^2 [8]

$$\delta_{i,a} - \delta_{o,a} \approx \delta_m^2\frac{T}{w}, \tag{9}$$

where $\delta_m = \tau_s\delta_s$ is the mean steer angle at wheels, with τ_s the steering ratio and δ_s the steering wheel angle. Clearly, δ_m is nearly identical to $\delta_i\delta_o$.

The different definitions are compared in Fig. 1b using the current FSAE steering layout. Application of (2) gives a (constant) Ackermann ratio of 47 % (green solid line with crosses). All the other definitions are almost coincident and equal to 32 % at very small wheel-steer angles. Definitions ν_w (3) and ν_n (4) with (6) remain very close in the whole steer range, raising from 32 % to 34 % (dashed violet and solid blue respectively). Definition ν_n (4) with (7) increases slightly more, and reaches a final value of 36 % (dotted yellow). Definition ν_n (4) with (5) is more sensitive to steer changes and raises to 40 % at the maximum steering considered (thick solid red). Definition ν_n (4) with (8) is decreasing to 29 % at the maximum steering angle, while definition ν_n (4) with (9) is almost constant. Finally, when applying a four-bar linkage with the two rockers pointing towards the middle of the rear axle, ratios in the range 24-33 % are obtained, depending on the definition selected.

Summarising, the net-steer definitions should be preferred over the practical ones, such as those related to the intersection of the rocker axes. The definition (4) with (6) is the one preferred by the authors.

3. Numerical model

A standard double-track model has been employed for the optimal control problem (OCP) with the different steering layouts. The roll, pitch and bounce degrees of freedom are neglected, together with the suspension travels. Similar models have been used in [2, 5, 6, 19, 20]. In this formulation different left and right steering angles can be employed at the front wheels. The main model quantities are depicted in Fig. 4, while the model parameters are reported in Tab. 1. The dynamic equations are:

$$\begin{aligned}
ma_x &= F_{xfl}\cos\delta_{fl} + F_{xfr}\cos\delta_{fr} - F_{yfl}\sin\delta_{fl} - F_{yfr}\sin\delta_{fr} + \\
&\quad F_{xrl}\cos\delta_{rl} + F_{xrr}\cos\delta_{rr} - F_{yrl}\sin\delta_{rl} - F_{yrr}\sin\delta_{rr} - F_D, && (10)\\
ma_y &= F_{xfl}\sin\delta_{fl} + F_{xfr}\sin\delta_{fr} + F_{yfl}\cos\delta_{fl} + F_{yfr}\cos\delta_{fr} + \\
&\quad F_{xrl}\sin\delta_{rl} + F_{xrr}\sin\delta_{rr} + F_{yrl}\cos\delta_{rl} + F_{yrr}\cos\delta_{rr}, && (11)\\
0 &= mg + F_{Lf} + F_{Lr} - N_{fl} - N_{fr} - N_{rl} - N_{rr}, && (12)\\
ma_y h &= \frac{T}{2}(N_{fl} - N_{fr} + N_{rl} - N_{rr}), && (13)\\
ma_x\, h &= aF_{Lf} - bF_{Lr} - a(N_{fl} + N_{fr}) + b(N_{rl} + N_{rr}), && (14)\\
I_z\dot{\Omega} &= \frac{T}{2}\left(F_{xfl}\cos\delta_{fl} - F_{xfr}\cos\delta_{fr} - F_{yfl}\sin\delta_{fl} + F_{yfr}\sin\delta_{fr}\right) - \\
&\quad \frac{T}{2}\left(F_{xrl}\cos\delta_{rl} + F_{xrr}\cos\delta_{rr} - F_{yrl}\sin\delta_{rl} - F_{yrr}\sin\delta_{rr}\right) + \\
&\quad a\left(F_{xfl}\sin\delta_{fl} + F_{xfr}\sin\delta_{fr} + F_{yfl}\cos\delta_{fl} + F_{yfr}\cos\delta_{fr}\right) - \\
&\quad b\left(F_{xrl}\sin\delta_{rl} + F_{xrr}\sin\delta_{rr} + F_{yrl}\cos\delta_{rl} + F_{yrr}\cos\delta_{rr}\right), && (15)
\end{aligned}$$

where the first three equations represent the force balance along the longitudinal, lateral and vertical direction respectively, while the latter three equations represent the moment balance around the roll, pitch and yaw axes through the projection of the center of mass on the ground. In (10) and (14), the longitudinal acceleration is $a_x = \dot{u} - \Omega v$, where u and v are the longitudinal and lateral velocity of the vehicle respectively ($V = \sqrt{u^2 + v^2}$ is the total velocity), while Ω is the yaw rate. In (11) and (13), the lateral acceleration is $a_y = \dot{v} + \Omega u$. The aerodynamic forces consist of the drag force F_D and the front F_{Lf} and rear F_{Lr} downforces. They are applied on the road plane (see Fig. 4), and are given by

$$F_D = \frac{1}{2}\,\rho_a\, C_D A\, u^2, \qquad F_{Lf} = \frac{1}{2}\,\rho_a\, C_{Lf} A\, u^2, \qquad F_{Lr} = \frac{1}{2}\,\rho_a\, C_{Lr} A\, u^2. \tag{16}$$

The tyre longitudinal and lateral forces are given by F_{xij} and F_{yij} respectively, where $i = f, r$ (front, rear) and $j = l, r$ (left, right). The tyre forces are computed employing

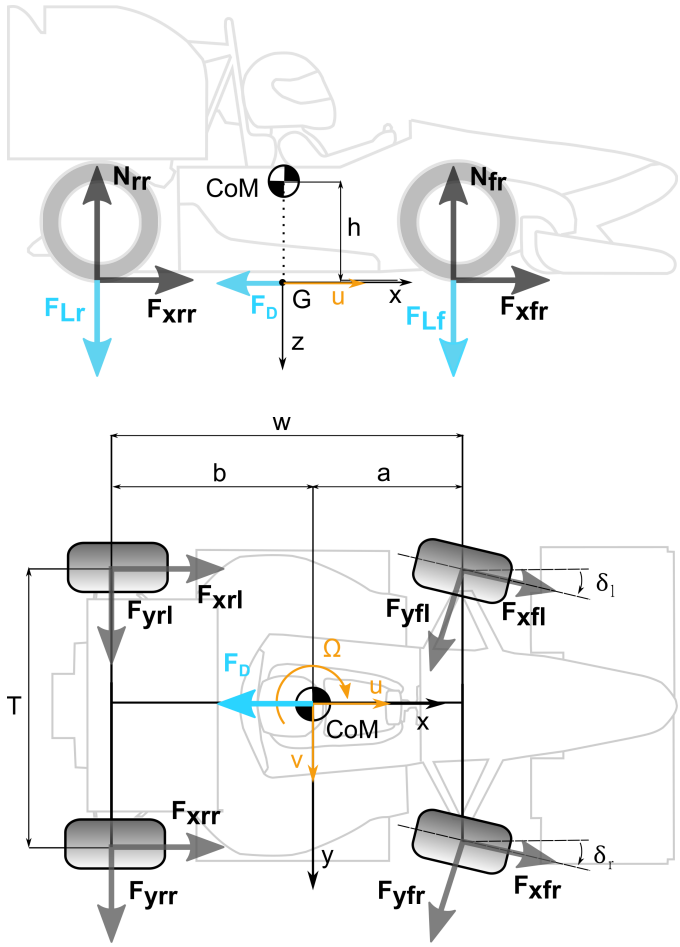

Figure 4.: Car model.

the Magic Formula with theoretical slips [34]:

$$F_x = N\,\frac{\sigma_x}{\sigma}\,D_x \sin\{C_x \arctan\left[B_x\,\sigma - E_x\left(B_x\,\sigma - \arctan(B_x\,\sigma)\right)\right]\}, \tag{17}$$

$$F_y = N\,\frac{\sigma_y}{\sigma}\,D_y \sin\{C_y \arctan[B_y\,\sigma - E_y\left(B_y\,\sigma - \arctan(B_y\,\sigma)\right)]\} + SV_y, \tag{18}$$

with

$$\sigma_x = \frac{\kappa}{1+\kappa}, \quad \sigma_y = \frac{\tan(\lambda)}{1+\kappa}, \quad \sigma = \sqrt{\sigma_x^2 + \sigma_y^2}, \tag{19}$$

where the theoretical slips σ_x, σ_y and σ are computed from the longitudinal and lateral (practical) slips κ and λ [34]:

$$\lambda_{fl} = \delta_{fl} - \frac{v + \Omega a}{u + \frac{T}{2}\Omega}, \qquad \lambda_{fr} = \delta_{fr} - \frac{v + \Omega a}{u - \frac{T}{2}\Omega}, \tag{20}$$

$$\lambda_{rl} = \delta_{rl} - \frac{v - \Omega b}{u + \frac{T}{2}\Omega}, \qquad \lambda_{rr} = \delta_{rr} - \frac{v - \Omega b}{u - \frac{T}{2}\Omega}. \tag{21}$$

The steering angles on each wheel δ_{ij}, where $i = f, r$ (front, rear) and $j = l, r$ (left, right), can be computed as

$$\delta_{fl} = \delta_l - \tau_f, \qquad \delta_{fr} = \delta_r + \tau_f, \tag{22}$$

$$\delta_{rl} = -\tau_r, \qquad \delta_{rr} = \tau_r, \tag{23}$$

where δ_l and δ_r are the left and right wheel-steering angles in a zero-toe configuration, while τ_f and τ_r are the toe angles at the front and rear tyres respectively (positive for toe-out). The longitudinal slip will be an input to the model. Finally, B, C, D and E are the Pacejka's coefficients, which are herein expressed in the simplified form introduced in [16, 18]. The purpose is to avoid the full Magic Formula formulation, while retaining some of its key features, namely load dependent friction coefficients, load-dependent position of the peak of the force vs. slip curves, and load dependent cornering stiffness per unit load. The coefficients are

$$K_x = B_x\, C_x\, D_x = N\, pK_{x1} \exp(pK_{x3}\, df_z), \tag{24}$$

$$E_x = pE_{x1}, \tag{25}$$

$$D_x = (pD_{x1} + pD_{x2}\, df_z)\, \lambda_{\mu,x}, \tag{26}$$

$$C_x = pC_{x1}, \tag{27}$$

$$B_x = \frac{K_x}{C_x\, D_x\, N}, \tag{28}$$

$$K_y = N_0\, pK_{y1}\, \sin\left(2\, \arctan \frac{N}{pK_{y2}\, N_0}\right), \tag{29}$$

$$E_y = pE_{y1}, \tag{30}$$

$$D_y = (pD_{y1} + pD_{y2}\, df_z)\, \lambda_{\mu,y}, \tag{31}$$

$$C_y = pC_{y1}, \tag{32}$$

$$B_y = \frac{K_y}{C_y\, D_y\, N}, \tag{33}$$

$$SV_y = N(pV_{y3} + pV_{y4} df_z)\phi\lambda_{\mu,y}, \tag{34}$$

where $df_z = (N - N_0)/N_0$, N_0 is a reference load and ϕ is the wheel-camber angle. A positive camber angle produces negative forces on the right tyres and positive forces on the left tyres, i.e. the top of the tyres are farther from the vehicle. The dataset of tyre parameters is given in Tab. 1 and the related characteristics are plotted in Fig. 12. The tyre normal forces are given by N_{ij}, where again $i = f, r$ and $j = l, r$ (see Fig. 4), and are computed from the system consisting of (12), (13) and (14), with the roll stiffness balance

$$ma_y \frac{h}{T}\xi = \frac{N_{fl} - N_{fr}}{2}, \tag{35}$$

where $\xi = K_{\phi f}/(K_{\phi f} + K_{\phi r})$ is the roll stiffness ratio, $K_{\phi f}$ is the front-axle roll stiffness, and $K_{\phi r}$ is the rear-axle roll stiffness. The total driving force F_x is split between the rear and front axle according to the distribution factor k_t, under the open-differential

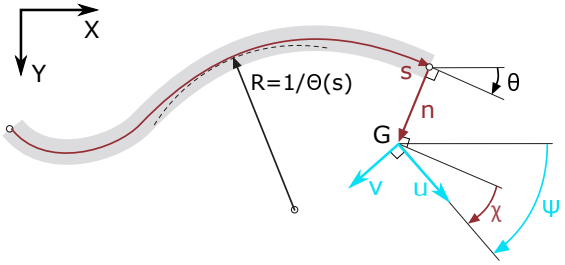

Figure 5.: Curvilinear coordinates.

assumption:

$$F_{xfl} = \frac{(1-k_t)F_x}{2}, \qquad F_{xfr} = \frac{(1-k_t)F_x}{2}, \tag{36}$$

$$F_{xrl} = \frac{k_t F_x}{2}, \qquad F_{xrr} = \frac{k_t F_x}{2}. \tag{37}$$

During acceleration $k_t = 1$ for rear-wheel-drive (RWD) vehicles, $k_t = 0$ for front-wheel-drive (FWD) vehicles, and $0 < k_t < 1$ for all-wheel-drive (AWD) vehicles. During braking the distribution factor is given by

$$k_t = \frac{1}{1+\gamma}, \qquad \gamma = \frac{F_{xfl} + F_{xfr}}{F_{xrl} + F_{xrr}}, \tag{38}$$

where γ is the brake ratio, which is here defined as the ratio between the front and rear longitudinal tyre forces – the switch between the value of k_t in acceleration and the value of k_t in braking is implemented through an approximation of a piecewise function, in order to avoid numerical issues.

The position of the vehicle on the road is described by the absolute motion of the road-centre-line frame, given by

$$\dot{s} = \frac{u\cos\chi - v\sin\chi}{1 - n\Theta}, \tag{39}$$

$$\dot{n} = u\sin\chi + v\cos\chi, \tag{40}$$

$$\dot{\chi} = \Omega - \Theta\frac{u\cos\chi - v\sin\chi}{1 - n\Theta}, \tag{41}$$

where s is the curvilinear coordinate of the road centre-line, n is the lateral position of the vehicle and χ is the angle between the tangent to the centre-line and the vehicle absolute speed (see Fig. 5).

4. Nonlinear optimal control

A nonlinear optimal control method is employed for simulating the dynamics of the nonlinear car model and assessing the performance with the different steering layout. The optimal control problem (OCP) aims to minimise a target function, while satisfying the state-space equations of the model $\dot{\mathbf{x}} = \mathbf{f}(\mathbf{x}, \mathbf{u})$, together with a certain number of

equality and inequality constraints. The state and control vectors are defied as:

$$\mathbf{x} = [u, v, \Omega, n, \chi]^T, \tag{42}$$

$$\mathbf{u} = [\delta_l, \delta_r, N_{fl}, N_{fr}, N_{rl}, N_{rr}, \kappa_{fl}, \kappa_{fr}, \kappa_{rl}, \kappa_{rr}]^T, \tag{43}$$

where δ_l is the steering angle of the left wheel, δ_r is the steering angle of the right wheel, N_{ij} and κ_{ij} are the loads and slips of the four tyres. The state-space equations of the dynamic system are (10), (11), (15), (39)-(41), while (12), (13) and (14) represent the problem constraints, together with (35) and (36)-(37). Additional constraints are included to account for the limited steering angle and steering angle rate

$$|\delta| \leq \delta_{\max}, \qquad |\dot{\delta}| \leq \dot{\delta}_{\max}, \tag{44}$$

for the limited longitudinal slip rate

$$|\dot{\kappa}| \leq \dot{\kappa}_{\max}, \tag{45}$$

and for the limited engine power

$$F_x u \leq P_{\max}, \tag{46}$$

where F_x is the total driving force. It is assumed that there is no limit on the maximum braking force, i.e. the brake system can always provide the necessary braking power. An additional constraint for the steering angle is included to simulate the fixed steering geometry:

$$\delta_l = \delta_l(\delta_r), \tag{47}$$

i.e. the left steer angle is a function of the right steering angle, e.g. according to the Ackermann steering, the parallel steering, etc. Finally, the vehicle is constrained to move within the road borders

$$-r_{wl} \leq n \leq r_{wr}, \tag{48}$$

where r_{wl} and r_{wr} represent the left and right road limits.

It is well known [2] that the model can be conveniently rewritten in the space domain

$$\mathbf{x}' = \frac{d\mathbf{x}}{ds} = \frac{\dot{\mathbf{x}}}{\dot{s}}, \tag{49}$$

where $\dot{s}$ is computed from (39).

The target $\mathcal{J}$ of the OCP is the manoeuvre time, which can be computed from the speed along the centre-line as follows

$$\mathcal{J} = \int dt = \int \frac{1}{\dot{s}}\, ds. \tag{50}$$

A direct collocation method is employed for the numerical solution of the OCP [14, 35], while automatic differentiation is used to speed-up the computation [36]. The error

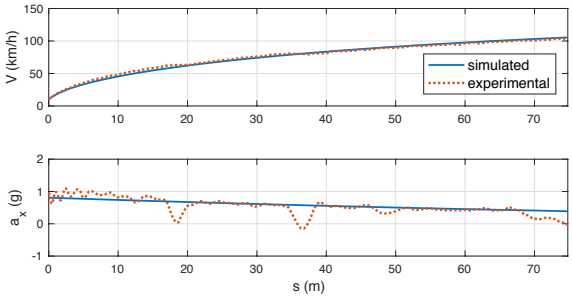

Figure 6.: Acceleration: experimental and simulated speed (top) and longitudinal acceleration (bottom).

tolerance for the mesh refinement is 10^{-4}, with respect to the scaled state variables; the error tolerance for the NLP solver is 10^{-7}.

5. Validation

The numerical simulations have been compared against the experimental data in three manoeuvres: acceleration, skidpad and slalom. The first two tests have been performed within the 2018 Italian FSAE competition in Varano de' Melegari (PR), while the slalom manoeuvre is a benchmark for the autocross and endurance tests. The vehicle is provided with a Plex VMU-900 IMU for measuring chassis accelerations and angular velocities, two rotary potentiometers Avio Race Hall AR 006-10 for measuring the steering angle and the throttle pedal position, four linear potentiometers DIA 9,5-75 mounted on each spring-damper assembly for measuring the suspension travel and rate, and four wheel-speed sensors (Texsense M10).

5.1. *Acceleration*

The acceleration test is performed on a 75 m straight road, where the target is obviously to reach the finish line in the minimum time. The simulation starts at a speed of 10 km/h, and reaches the speed of 100 km/h in 64 m. In the experimental data the same speed is reached in 66 m (Fig. 6). The speed profiles are almost identical, although the gear change (see acceleration drops at 18 m and 37 m) is not included in the numerical model.

5.2. *Skidpad*

The skidpad test consists in performing steady turning manoeuvres of given radius, at the maximum speed. The actual track geometry has an eight-shaped pattern, with an average curvature radius of 9.1 m and a width of 3.0 m. The driver has to perform two clockwise turns on the first circle of the eight and two counter-clockwise turns on the second circle. Since the vehicle numerical model is symmetric with respect to its vertical plane, only the clockwise turns can be considered – results on the counter-clockwise turns are clearly identical. In the OCP simulation the car enters the skidpad course and keeps turning for three turns. Steady-state conditions are reached after one turn. In steady state conditions the numerical driver has no oscillations on the steer and throttle inputs, differently from the real driver who is always adjusting the control inputs while trying to

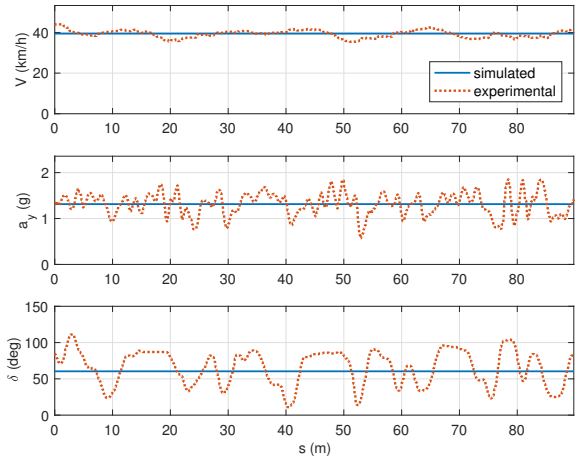

Figure 7.: Skidpad: experimental and simulated speed (top), lateral acceleration (centre), steering wheel angle (bottom).

keep the car close to its physical limit. In the road tests the mean speed is 39 km/h, with a mean lateral acceleration of 1.34 g, a mean steering wheel angle of 62 deg (mean wheel angle of 10.7 deg); see Figure 7. In the OCP simulation the speed is limited to 39 km/h (same as the real road test) and the vehicle turns with a lateral acceleration of 1.31 g and a steering wheel angle of 60 deg (mean wheel angle of 10.3 deg).

The skidpad test is then repeated at speeds between 10 and 15 km/h and the steering angle vs. lateral acceleration profile is obtained. The slope of this profile (i.e. the understeer gradient) for lateral accelerations between 0.1 and 0.2 g is 0.943 deg/g.

5.3. *Slalom*

The slalom course consists of four cones, at a distance of 12.4 m: the target is turning around the cones in the minimum time. This path emulates sections of the autocross and endurance FSAE tracks, and represents an important benchmark for assessing the handling of the car. The experimental manoeuvre is obtained using the speed limiter at

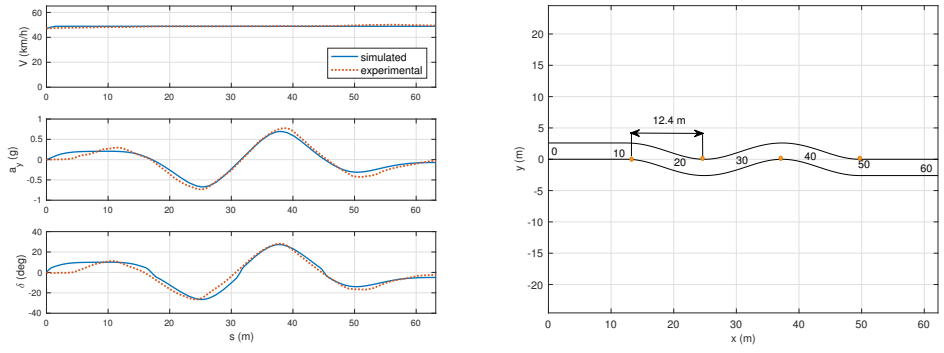

(a) (b)

Figure 8.: Slalom. a) Experimental and simulated speed (top), lateral acceleration (centre), steering wheel angle (bottom). b) Slalom course.

49 km/h: the same speed is set as upper bound for the speed in the OCP simulation. In order to perform a slalom manoeuvre within the minimum time OCP framework, a S-shaped track is built, in which the corner apexes mimic the position of the cones, see Figure 8b. Since the OCP aims at moving the vehicle close to the apexes for the best performance, the width of the track has no effect on the results. A cosine function is employed to build the S-shaped track. Initial and final straights of 12.5 m are included. In the measured data, the vehicle travels at 49 km/h, while the lateral acceleration is in the range ±0.8 g and the steering wheel angle in the range ±28 deg (±4.6 deg at wheels) see Figure 8. The OCP simulation results are consistent with the experimental data: the lateral acceleration is in the range ±0.7 g, the steering wheel angle is in the range ±28 deg (±4.6 deg at wheels).

6. Effect of steering

In this section, the effect of the steering geometry will be analysed employing the vehicle model validated in the previous section. Three different steering strategies will be considered (baseline, Ackermann and parallel) together with three different manoeuvres (skidpad, slalom and racetrack). Before starting the analysis, the understeer gradient will be calculated for each steering configuration through a series of steady-turning manoeuvres at different speeds. Toe and camber angles are set to zero, in order to isolate the effect of steering geometry.

6.1. *Steering characteristics*

The understeer gradient is obtained from steady-state tests at different speeds. The OCP simulation is run with the same procedure described for the skidpad, Section 5.2. The vehicle travels a constant-radius corner ($R = 50$ m), while the speed spans from 15 km/h to 100 km/h. The manoeuvre is consistent with the international standard [37].

The understeer gradient, computed as the slope of the steering angle vs. lateral acceleration between 0.1 and 0.2 g [38], is 0.021 deg/g for the baseline vehicle, 0.026 deg/g in case of Ackermann steering geometry and 0.019 deg/g for parallel steering.

The Ackermann steering vehicle is the most understeering, followed by the baseline and the parallel. However, it can be verified that, as expected, the Ackermann configuration requires the minimum steering angle at very low speeds.

The understeer gradients may seem quite small. This is because toe and camber angles are neglected. In the case the toe angle is included, the values raise significantly. With the baseline vehicle and a 2 deg toe-out at the front, the understeer gradient raises to 2.761 deg/g, while with a 2 deg toe-in at the front, the understeer gradient raises to 0.458 deg/g. Therefore, with the selected dataset, (front) toe-out gives more understeering than (front) toe-in. In the current model toe angles are not dependent on lateral load transfer and suspension structural compliance. With 2 deg camber-in at the front wheels the understeer gradient reduces to -0.047 deg/g, while with 2 deg camber-out the understeer gradient (slightly) increases to 0.089 deg/g. Therefore, the camber-in configuration is less understeering than the camber-out. These figures need be compared with 0.021 deg/g, which is computed in the case of zero toe and zero camber and shows that the effect of toe is the most significant on the steering characteristic. Finally, in the case toe and camber of the skidpad configuration are included, the understeer gradients are 1.144 deg/g for baseline, 1.157 deg/g for Ackermann and 1.138 deg/g for parallel; again, the values get larger but the ranking of configurations remains the same.

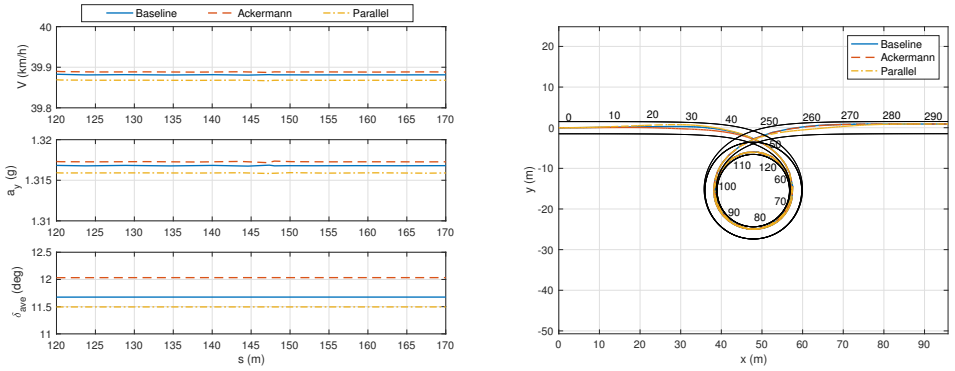

(a) (b)

Figure 9.: Skidpad. a) Speed, lateral acceleration and average steering angle during steady-turning. b) Track and trajectory.

6.2. *Skidpad*

The skidpad manoeuvre is now examined to assess the maximum performance of the different steering configurations. The same course used in Sec. 5.2 is considered.

In Fig. 9a the speed, lateral acceleration and average steer angle at the wheels are shown during the steady-turning part of the skidpad manoeuvre (for travelled distance from 120 m, i.e. after one turn of the circle, to 170 m, i.e. before exiting the circle; see Fig. 9b). The speed is 39.88 km/h for the baseline, 39.89 km/h for Ackermann (fastest) and 39.87 km/h for parallel (slowest). The corresponding lateral accelerations are 1.317 g, 1.317 g and 1.316 g respectively, while the average steering angles at wheels are 11.68 deg, 12.03 deg and 11.50 deg.

Overall, the effect of the steering geometry is very small on the maximum speed achievable (0.05 %). However, the related steering gradients ($R = 9.1$ m) are quite different: -0.117 deg/g for the baseline, -0.041 deg/g for Ackermann and -0.136 deg/g for parallel – all oversteering. It is worth noting that the understeer gradients are all positive (i.e. understeering behaviour) when computed on a turn with $R = 50$ m. However, the understeer ranking of configuration is the same: Ackermann, baseline and parallel.

In conclusion, a slightly larger steady-turning lateral acceleration (in the case of zero toe and zero camber) is achieved with the Ackermann configuration, which is also the least oversteering.

However, when toe and camber are included (as for validation), the speed raises to 44.36 km/h in the case of the baseline configuration, to 44.33 km/h in the case of Ackermann and to 44.40 km/h (fastest, by 0.16 %) in the case of parallel steering. The corresponding lateral acceleration are 1.662 g, 1.661 g and 1.667 g respectively, while the average wheel steering angles are 10.6 deg, 11.01 deg and 10.4 deg. Therefore the most performing configuration is the parallel one.

The different steering configurations are also associated to different tyre drag forces, because different sideslips are engaged. In the case no toe and no camber are included, the induced drag forces amount to 88 % of the total longitudinal (propulsive) force, while differences in the induced drag forces are within 0.15 %. In the case camber and toe are included, the induced forces raise to 91 % of the total longitudinal force, and differences in the induced forces are up to 1.5 %. Differences in the total longitudinal forces are below 1 % when no toe and camber are considered, while they raise to 2-4 % in the case toe and camber are included.

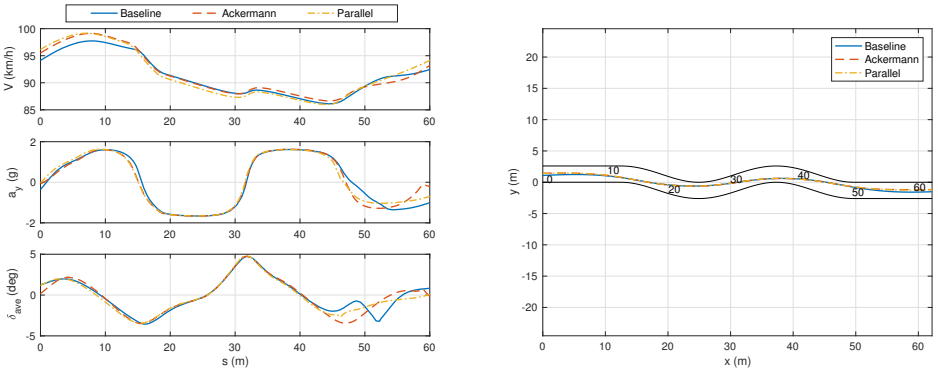

(a) (b)

Figure 10.: Slalom. a) Speed, lateral acceleration and average steering angle. b) Vehicle trajectory.

6.3. *Slalom*

The slalom manoeuvre is performed on the same course used in Sec. 5.3 for the model validation, see Fig. 10b. The speed is constrained to assume the same values at the beginning and at the end of the slalom course (cyclic condition). No constraints are employed for limiting the speed to a constant value.

The maximum lateral acceleration is 1.658 g for the baseline, 1.663 g for Ackermann (highest) and 1.658 g for the parallel steering configuration. The maximum average wheel-steering-angle is 4.73 deg for baseline (lowest), 4.74 deg for Ackermann and 4.82 deg for parallel (highest), see Fig. 10a.

The manoeuvre time is 2.468 s for the baseline (slowest), 2.457 s for Ackermann (fastest) and 2.461 s for parallel. The maximum difference among the different configurations is 11 ms (0.4%). The Ackermann configuration is again the best, in the case of zero toe and zero camber.

When including toe and camber (as for validation) the manoeuvre times reduces to 2.130 s for the baseline, 2.130 s for Ackermann and 2.129 s (fastest, although almost identical to the previous configurations) for the parallel.

Similarly to the skidpad scenario, also in the slalom the different steering configurations are associated to different tyre drag forces. The maximum induced forces amount to 7 % when toe and camber are neglected, while they raise to 13 % when toe and camber are included. These figures are much smaller than those of the skidpad, where much larger steering angles are involved. The differences in the induced drag forces are in the range 2-4 %.

6.4. *Racetrack*

The different steering geometries are simulated also on a lap of the Adria International Raceway (Italy), characterised by a total length of 2702 m, and eight turns mainly paced at speeds below 80 km/h, see Fig. 11. The vehicle travels the track anticlockwise and reaches a maximum speed of ∼154 km/h at the pit-straight, while the minimum speed is ∼58 km/h at turn 3. The maximum lateral acceleration is ∼2.1 g at turn 4. More precisely, the maximum speed (pit-straight) is 154.55 km/h for baseline (fastest), 154.54 km/h for Ackermann, 154.51 km/h for parallel (slowest). The minimum speed (turn 3) is 58.69 km/h for baseline (fastest), 58.65 km/h for Ackermann, 58.62 km/h

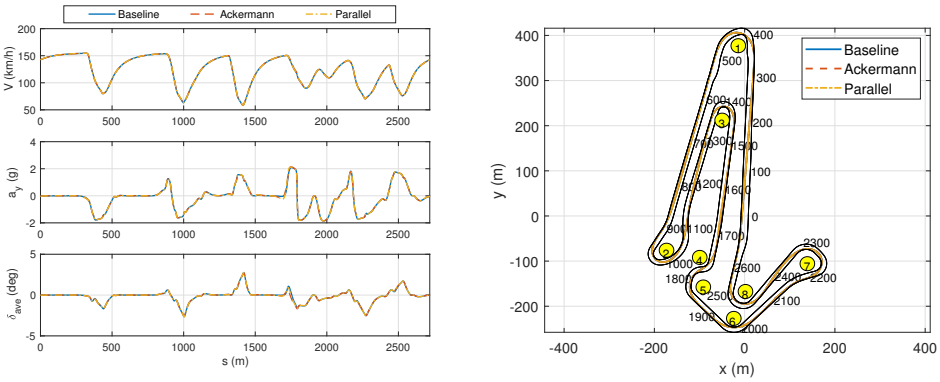

(a) (b)

Figure 11.: Racetrack. a) Speed, lateral acceleration and average steering angle. b) Racetrack and trajectory.

for parallel (slowest). The maximum lateral acceleration (turn 4) is 2.147 g for baseline (highest), 2.146 g for Ackermann, 2.124 g for parallel (lowest). The lap-time is 82.853 s for baseline (slowest), 82.827 s for Ackermann, 82.827 s for parallel. The maximum difference among the different configurations is 26 ms (0.03%). The mean difference of the lateral positions on the road (variable n in Fig. 5) of the Ackermann and parallel configurations with respect to the baseline are 0.040 m and 0.070 m respectively.

When the toe and camber are included (as for the slalom validation). the lap time reduces to 79.173 s (slowest) for the baseline, 78.844 s (fastest) for Ackermann and 78.891 s for parallel. The lap time difference in this case raises to 329 ms (0.4 %), which is much larger than the difference obtained in the case the sole steering configuration is changed. The mean difference of the lateral positions on the road (variable n in Fig. 5) of the Ackermann and parallel configurations with respect to the baseline configuration are around 0.5 m in both cases, again an order of magnitude larger than the differences observed when varying the steering configuration only.

Finally, the maximum induced forces amount to 4 % of the total longitudinal propulsive force when toe and camber are neglected, while they raise to 10 % when toe and camber are included. Again, these figures are much smaller than those of the skidpad, where much larger steering angles are involved. The differences in the maximum induced drag forces are in the range 1-3 %.

7. Remarks

The analysis in sections 6 showed that the effect of the steering configuration is significantly smaller than the effect of toe and camber. The toe is the most influential parameter when it comes to performance of the vehicle under investigation. Indeed the magnitude of the toe angle employed (around 2 deg) is comparable with the typical average wheel steering angle during a lap of the selected racetrack, more than one-half of the wheel steering angle employed during the slalom and about one-fourth of the steering angle employed during the skidpad.

8. Conclusions

The work reviewed the different definitions of Ackermann steering ratio and investigated the effect of the steering geometry on the performance of a race car. The model of a Formula SAE car has been built and validated against experimental data. The effect of the baseline geometry, a pure Ackermann geometry and a parallel steering geometry has been assessed in skidpad, slalom and a lap of the Adria International Raceway, employing nonlinear optimal control techniques. It has been found that the effect of the Ackermann ratio on the maximum performance is small, at least when compared with the effect of toe, whose magnitude can be comparable with the wheel steering angle on a racetrack.

Acknowledgements

The authors acknowledge the support of Prof. G. Meneghetti and the FSAE RaceUp team of the University of Padova.

References

[1] King-Hele D. Erasmus darwin's improved design for steering carriages—and cars. Notes and records of the Royal Society of London. 2002;56(1):41–62.
[2] Limebeer DJN, Massaro M. Dynamics and optimal control of road vehicles. Oxford University Press; 2018.
[3] Lincoln C. Steering mechanisms and how they got that way. SAE Technical Paper; 1956. Report no.:.
[4] Genta G, Morello L, Cavallino F, Filtri L. The motor car: Past, present and future. Springer Science & Business Media; 2014.
[5] Jazar RN. Vehicle dynamics: theory and application. Springer; 2017.
[6] Gillespie TD. Fundamentals of vehicle dynamics. SAE International; 1992.
[7] Milliken WF, Milliken DL, et al. Race car vehicle dynamics. Vol. 400. Society of Automotive Engineers Warrendale; 1995.
[8] Guiggiani M. The science of vehicle dynamics: Handling, braking, and ride of road and race cars. Springer; 2018.
[9] Wolfe W. Analytical design of an ackermann steering linkage. Journal of Engineering for Industry. 1959;81(1):10–13.
[10] Miller GR. The effect of ackerman steering correction upon front tire wear of medium duty trucks. SAE Technical Paper; 1986. Report no.:.
[11] Simionescu P, Beale D. Optimum synthesis of the four-bar function generator in its symmetric embodiment: the ackermann steering linkage. Mechanism and Machine Theory. 2002;37(12):1487–1504.
[12] Mitchell WC, Staniforth A, Scott I. Analysis of ackermann steering geometry. SAE Technical Paper. 2006;.
[13] Farazandeh A, Ahmed A, Rakheja S. Performance enhancement of road vehicles using active independent front steering (aifs). SAE International journal of passenger cars-mechanical systems. 2012; 5(2012-01-2013):1273–1284.
[14] Dal Bianco N, Bertolazzi E, Biral F, Massaro M. Comparison of direct and indirect methods for minimum lap time optimal control problems. Vehicle System Dynamics. 2018;0(0):1–32.
[15] Massaro M, Marconi E. The effect of engine spin direction on the dynamics of powered two wheelers. Vehicle System Dynamics. 2018;56(4):604–620.
[16] Veneri M, Massaro M. A free-trajectory quasi-steady-state optimal-control method for minimum lap-time of race vehicles. Vehicle System Dynamics. 2019;:1–22.
[17] Tremlett A, Limebeer DJN. Optimal tyre usage for a formula one car. Vehicle System Dynamics. 2016;54(10):1448–1473.
[18] Tremlett A, Massaro M, Purdy D, Velenis E, Assadian F, Moore A, Halley M. Optimal control of motorsport differentials. Vehicle System Dynamics. 2015;53(12):1772–1794.

[19] Perantoni G, Limebeer DJN. Optimal control for a formula one car with variable parameters. Vehicle System Dynamics. 2014;52(5):653–678.
[20] Limebeer DJN, Perantoni G, Rao AV. Optimal control of formula one car energy recovery systems. International Journal of Control. 2014;87(10):2065–2080.
[21] Masouleh MI, Limebeer DJN. Optimizing the aero-suspension interactions in a formula one car. IEEE Transactions on Control Systems Technology. 2016 May;24(3):912–927.
[22] Tavernini D, Velenis E, Lot R, Massaro M. The optimality of the handbrake cornering technique. Journal of Dynamic Systems, Measurement, and Control. 2014;136(4).
[23] Tavernini D, Massaro M, Velenis E, Katzourakis D, Lot R. Minimum time cornering: The effect of road surface and car transmission layout. Vehicle System Dynamics. 2013;51(10):1533–1547.
[24] Bobbo S, Cossalter V, Massaro M, Peretto M. Application of the optimal maneuver methodî for enhancing racing motorcycle performance. SAE International Journal of Passenger Cars-Mechanical Systems. 2009;1(1):1311–1318.
[25] Kelly DP. Lap time simulation with transient vehicle and tyre dynamics [dissertation]. Cranfield University; 2008.
[26] Bertolazzi E, Biral F, Da Lio M. Symbolic-numeric efficient solution of optimal control problems for multibody systems. Journal of computational and applied mathematics. 2006;185(2):404–421.
[27] Casanova D, Sharp RS, Symonds P. Minimum time manoeuvring: The significance of yaw inertia. Vehicle system dynamics. 2000;34(2):77–115.
[28] Casanova D. On minimum time vehicle manoeuvring: The theoretical optimal lap [dissertation]. School of Engineering, Cranfield University; 2000.
[29] Cossalter V, Da Lio M, Lot R, Fabbri L. A general method for the evaluation of vehicle manoeuvrability with special emphasis on motorcycles. Vehicle system dynamics. 1999;31(2):113–135.
[30] Hendrikx J, Meijlink T, Kriens R. Application of optimal control theory to inverse simulation of car handling. Vehicle System Dynamics. 1996;26(6):449–461.
[31] BS-ISO-8855:2011. Road vehicles–vehicle dynamics and road-holding ability–vocabulary. International Organization for Standardization; 2011. Standard.
[32] Burgess M, Fleming N, Wootton M, Williams S. A tool for rapid vehicle suspension design. SAE Technical Paper. 2004;.
[33] Lotus-Engineering. Lotus SHARK manual; 2004. Software manual.
[34] Pacejka H, Besselink I. Tire and vehicle dynamics. Elsevier Science; 2012.
[35] Patterson MA, Rao AV. GPOPS-II: A MATLAB software for solving multiple-phase optimal control problems using hp-adaptive gaussian quadrature collocation methods and sparse nonlinear programming. ACM Transactions on Mathematical Software (TOMS). 2014;41(1):1.
[36] Weinstein MJ, Rao AV. Algorithm 984: Adigator, a toolbox for the algorithmic differentiation of mathematical functions in matlab using source transformation via operator overloading. ACM Trans Math Softw. 2017 Aug;44(2):21:1–21:25.
[37] BS-ISO-4138:2012. Passenger cars - steady-state circular driving behaviour – open-loop test methods. International Organization for Standardization; 2012. Standard.
[38] Tandy DF, Colborn J, Bae JC, Coleman C, Pascarella R. The true definition and measurement of oversteer and understeer. SAE International Journal of Commercial Vehicles. 2015;8(2015-01-1592):160–181.

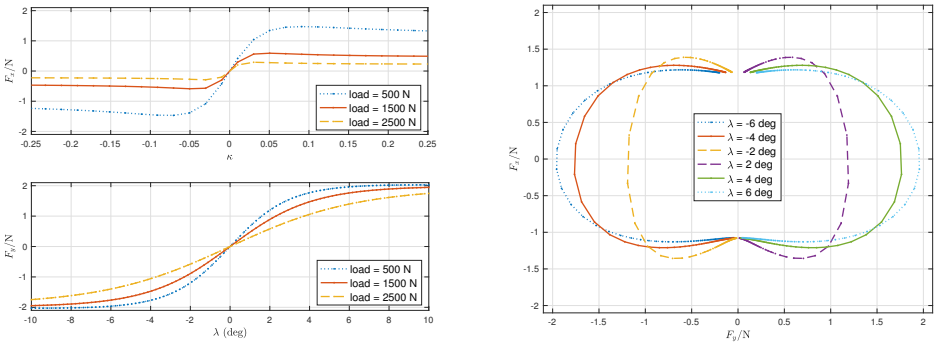

(a) (b)

Figure 12.: Longitudinal force F_x and lateral force F_y as a function of longitudinal slip κ and sideslip λ at zero camber: pure slip condition at different normal loads (a) and combined slip condition at 500 N (b). Tyre parameters are given in Tab. 1.

Table 1.: Baseline car parameters and tyre coefficient.

Symbol	**Description**	**Value**
g	gravity	$9.81\,\mathrm{m/s^2}$
ρ_a	air density	$1.20\,\mathrm{kg/m^3}$
m	mass	$280\,\mathrm{kg}$
h	height of CoM	$0.315\,\mathrm{m}$
w	wheelbase	$1.535\,\mathrm{m}$
a	CoM from front axle	$0.767\,\mathrm{m}$
b	CoM from rear axle	$0.768\,\mathrm{m}$
ξ	roll stiffness ratio	0.489
I_z	yaw inertia	$109\,\mathrm{kgm^2}$
T_f	front track	$1.220\,\mathrm{m}$
T_r	rear track	$1.190\,\mathrm{m}$
T	$(T_f + T_r)/2$	$1.205\,\mathrm{m}$
$C_D A$	drag area coefficient	$1.38\,\mathrm{m^2}$
$C_{Lf} A$	front lift area coefficient	$0.89\,\mathrm{m^2}$
$C_{Lr} A$	rear lift area coefficient	$1.33\,\mathrm{m^2}$
$P_{\max}$	maximum power	$66.3\,\mathrm{kW}$
pC_{x1}	Longitudinal shape factor	2.31
pD_{x1}	Max longitudinal friction coefficient	-1.20
pD_{x2}	Max longitudinal friction coefficient	0.71
pE_{x1}	Longitudinal curvature factor	1.00
pK_{x1}	Max longitudinal stiffness coefficient	39.06
pK_{x2}	Max longitudinal stiffness coefficient	-0.32
pK_{x3}	Max longitudinal stiffness coefficient	-0.23
$\lambda_{\mu,x}$	Longitudinal friction scaling factor	1.00
pC_{y1}	Lateral shape facto	1.86
pD_{y1}	Max lateral friction coefficient	-2.48
pD_{y2}	Max lateral friction coefficient	0.06
pE_{y1}	Lateral curvature factor	0.93
pK_{y1}	Max cornering stiffness coefficient	53.91
pK_{y2}	Max cornering stiffness coefficient	2.57
pK_{y3}	Max cornering stiffness coefficient	3.95
pV_{y3}	Variation of shift with camber	-3.01
pV_{y4}	Variation of shift with camber and load	-1.51
$\lambda_{\mu,y}$	Lateral friction scaling factor	0.61
N_0	reference normal load (for $df = 0\,\mathrm{N}$)	$809\,\mathrm{N}$
Acceleration		
τ_f	toe angle at the front wheels (toe-in)	$-0.5\,\mathrm{deg}$
τ_r	toe angle at the rear wheels (toe-in)	$-0.5\,\mathrm{deg}$
ϕ_f	camber angle at the front wheels (camber-in)	$-3.0\,\mathrm{deg}$
ϕ_r	camber angle at the rear wheels (camber-out)	$0.5\,\mathrm{deg}$
Skidpad		
τ_f	toe angle at the front wheels (toe-out)	$2.0\,\mathrm{deg}$
τ_r	toe angle at the rear wheels (toe-in)	$-0.5\,\mathrm{deg}$
ϕ_f	camber angle at the front wheels (camber-in)	$-3.0\,\mathrm{deg}$
ϕ_r	camber angle at the rear wheels (camber-in)	$-1.5\,\mathrm{deg}$
Slalom		
τ_f	toe angle at the front wheels (toe-out)	$2.8\,\mathrm{deg}$
τ_r	toe angle at the rear wheels (toe-in)	$-0.5\,\mathrm{deg}$
ϕ_f	camber angle at the front wheels (camber-in)	$-1.5\,\mathrm{deg}$
ϕ_r	camber angle at the rear wheels	$0.0\,\mathrm{deg}$